Original Research

Bionanocomposite Films from Resilin-CBD Bound to Cellulose Nanocrystals

Amit Rivkin,[1] Tiffany Abitbol,[1,2] Yuval Nevo,[1] Ronen Verker,[3] Shaul Lapidot,[1] Anton Komarov,[4] Stephen C. Veldhuis,[3] Galit Zilberman,[5] Meital Reches,[6] Emily D. Cranston,[2] and Oded Shoseyov[1]

[1]*The Hebrew University of Jerusalem, Faculty of Agriculture, Department of Biochemistry, Rehovot, Israel*
[2]*McMaster University, Department of Chemical Engineering, Hamilton, Canada*
[3]*Soreq NRC, Space Environment Department, Yavne, Israel*
[4]*McMaster University, Department of Mechanical Engineering, Hamilton, Canada*
[5]*RD&E Division, Elbit Systems Electro-optics-Elop Ltd., Rehovot, Israel*
[6]*The Hebrew University of Jerusalem, Institute of Chemistry, Givat Ram, Israel*

Abstract

This research explores the properties of bionanocomposite films prepared by binding recombinant resilin-like protein (res) consisting of the exon 1 resilin sequence from Drosophila melanogaster *engineered to include a cellulose binding domain (CBD), to cellulose nanocrystals (CNCs). The optimal binding of res-CBD to CNCs was 1:5 by mass, and the resulting res-CBD-CNCs remained colloidally stable in water. Res-CBD-CNCs were solvent cast into transparent, free-standing films, which were more hydrophobic than neat CNC films, with water contact angles of 70–80° compared to 35–40° for the latter. In contrast to the multi-domain orientation typical of chiral nematic CNC films, res-CBD-CNC and CBD-CNC films exhibited long-range, uniaxial orientation that was apparently driven by the CBD moiety. Glycerol was studied as an additive in the films to determine whether the addition of a wet component to solvate the recombinant protein improved the mechanical properties of the res-CBD-CNC films. In comparison to the other films, res-CBD-CNC films were more elastic with added glycerol, demonstrating a range of 0.5–5 wt% (i.e., the films responded more elastically to a given strain and/or were less plastically deformed by a given mechanical load), but became less elastic with added glycerol between 0.5–5 wt%. Overall, films made of res-CBD-CNCs plus 0.5 wt% glycerol displayed improved mechanical properties compared to neat CNC films, and with an increase in toughness of 150% and in elasticity of 100%.*

Introduction

Resilin and cellulose nanocrystals (CNCs) have both received increasing attention in recent years due to their impressive, yet distinct set of mechanical properties and also to advances in the technologies necessary for their production.[1,2] Global commercialization of CNCs and impressive production rates relative to other types of nanoparticles have the potential to impact nanocomposite applications, such as in coatings and adhesives, which may benefit from the inclusion of a readily available, green-sourced, biocompatible nanoparticle that has been shown to lead to significant improvements in the mechanical performance of plastics, even at modest particle loadings.[3] Similarly, advances in bioengineering have provided scientists with the strategies needed to design recombinant proteins with specific functionality in mind, such as elastomeric recombinant proteins based on resilin, which can then be used to prepare well-defined biomaterials.[4,5]

Resilin was discovered in the early 1960s by Weis-Fogh, who derived the name of the rubbery protein from the Latin word *resilire,* which means to spring back.[6] Weis-Fogh identified resilin in the cuticle of winged insects where it exists in a lamellar composite structure, with thick resilin layers sandwiched between thin layers of chitin.[7] It has since been found in various arthropod organs that require a high degree of elasticity and resilience—for example it has been found within the sound-generating tymbal of cicadas, and the metathoracic femur of the flea.[8,9] The structure-property relationship of resilin from *Drosophila melanogaster* has been recently elucidated by the Kaplan group at Tufts University (Boston, MA); the ''soft,'' highly resilient (>90% resilience) unstructured exon I domain quickly responds to energetic inputs and transfers energy to the ''hard,'' less resilient (~65% resilience) exon III domain, which becomes more ordered due to β-turns and releases energy upon return to an unstructured state. In full-length natural resilin, exon I and exon III are linked by the chitin-binding exon II moiety.[10]

CNCs, first isolated by Rånby in 1949, are rod-shaped (5–10 nm in width ×50–400 nm in length, depending on source and preparation conditions), highly crystalline nanoparticles produced by the partial and controlled degradation of native sources of cellulose from plants, bacteria, or animals.[1,11–18] Resilin and CNCs share some properties, including overall hydrophilicity, resistance to dissolution in most solvents, heat stability (140°C for resilin and ~300°C for Na-form CNCs), optical transparency, and their natural roles as critical structural components within biological systems.[19,20] However, in terms of mechanical properties, resilin and CNCs are very different. The structure of resilin, essentially an amorphous, polymer hydrogel held together by

DOI: 10.1089/ind.2014.0026

di- and tri-tyrosine crosslinks, imparts near perfect rubberiness, whereas the highly crystalline, hydrogen-bonded structure of CNCs imparts strength and stiffness comparable to steel and Kevlar® (DuPont, Wilmington, DE).[21–23]

In 2001, Ardell and Andersen tentatively identified the precursor CG15920 gene for resilin in *D. melanogaster*, and in 2005, Elvin et al. reported the cloning and expression of the first exon (exon 1) of the *Drosophila* gene as a soluble protein in *Escherichia coli*.[24,25] In addition, a highly elastic and resilient rubber was formed by photocrosslinking the recombinant protein, further confirming the role of the repetitive motif in resilin elasticity.[25] From a protein-production point of view, it was later shown that lactose-induced fermentation in *E. coli* gave a 20-fold increase in protein yield compared to previous expression systems.[26] Qin et al. described the cloning, expression, and purification of resilin-chitin binding domain (6H-resChBD) proteins (exon 1), which laid the foundation for the resilin-cellulose binding domain (CBD) construct used in the current work.[27] Here, we refer to the exon 1 *D. melanogaster* resilin-CBD construct simply as res-CBD. Similar to natural resilin, crosslinked materials prepared from either resilin-ChBD (full length) or res-CBD (exon 1) recombinant proteins exhibit elastomeric properties.[21,27,28]

We describe herein materials based upon res-CBD and cellulose nanocrystals, with the resilin interaction with the CNCs mediated by a CBD (*Clostridium cellulovorans*) genetically engineered and fused to the C-terminal of the exon 1 from *D. melanogaster* resilin.[28] The binding of res-CBD to CNCs has been previously explored by our group; Rivkin et al. prepared crosslinked, rubbery materials from res-CBD-CNCs, and Verker et al. showed that res-CBD-CNCs could be directly inserted into a hydrophobic epoxy matrix, giving a 50% improvement in the Young's modulus and a higher elasticity compared to the neat epoxy.[28,29] Most examples of resilin-like polypeptide-based materials use the recombinant protein in a crosslinked state, whereas the current work uses proresilin—the protein precursor to the crosslinked material.[2,24] This is an important distinction, since it implies that any resilin-derived changes to the mechanical performance of the nanocomposite films are not related to elastomeric properties in a traditional macro-sense, but rather to the addition of a largely unstructured polymeric component with elastic features. The expectation of elasticity/resilience from uncrosslinked resilin-like proteins may be reasonable. For instance, Qin et al. reported 90% resilience for the uncrosslinked exon 1 protein from *D. melanogaster* by atomic force microscopy (AFM) force measurements on dry samples, compared to 93% resilience for the crosslinked counterpart.[21] Finally, we note that the nanocomposite presented in this work consists mainly of CNCs with the low loading addition of polymer-like filler (res-CBD), whereas traditionally studied CNC nanocomposites are mainly comprised of polymer.

Materials and Methods

Cellulose nanocrystals produced from the sulfuric acid hydrolysis of Avicel were provided by Melodea Ltd (Rehovot, Israel). Standard biochemical reagents—Dowex Marathon MR-3 mixed bed resin, Dowex Marathon C strong acid resin, and Sigmacote—were purchased from Sigma-Aldrich (St. Louis, MO). Avicel PH-200 microcrystalline cellulose was purchased from FMC Biopolymer Inc. (Philadelphia, PA), and recombinant CBD from *C. cellulovorans* was expressed in *E. coli* and purified as described previously.[30] The construction, expression, and purification of *D. melanogaster* 17 repeat exon 1 pro-resilin (referred to simply as res in this work) was described previously by Qin et al.[27]

CONDUCTOMETRIC TITRATION

To ensure complete deionization, the CNCs were first treated with mixed bed resin, followed by a treatment with acidic resin, as previously described.[2] The H-form CNCs (0.02 g, 0.5 wt%) were then combined with NaCl (1 mM, 150 mL) and titrated against dilute NaOH (2 mM). The equivalence point from titration was related to the percent sulfur (%S) by assuming that each proton detected was associated with a sulfate half-ester group on the surface of the CNCs.[31]

ZETA-POTENTIAL

Suspensions of CNCs and res-CBD-CNCs (0.1 wt%, pH 8) were used for zeta-potential and electrophoretic mobility measurements (Zeta Potential ZetaPlus Analyzer, Brookhaven Instruments, Holtsville, NY). The results are an average of 10 runs.

PARTICLE SIZE BY NANOSIGHT

Particle size was determined using a NanoSight system (Malvern, Worcestershire, UK), which analyzes particles by direct tracking and measurement of diffusion events. The mean size determination assumes a spherical particle shape, which does not apply to the rod-like CNCs. Nonetheless, this type of measurement is useful for comparison between samples. The results presented are the mean size from a representative run. Samples for NanoSight were prepared in the same way as for zeta-potential, but in this case the samples were diluted to 0.0001 wt%.

EXPRESSION OF 6H-17-RESILIN-CBD

A lysogeny broth-agar plate containing ampicillin (100 mg/L) was streaked with a glycerol stock of BL-21 (DE3) bacteria containing the expression vector pHis-parallel3_17-res-CBD and incubated overnight (37°C). For the construction of the pHis-parallel3_17-res-CBD expression vector, see Rivkin et al.[28] A single colony was used for the inoculation of M9 minimal media (200 mL) containing glucose (0.8% w/v) and ampicillin (100 mg/L). The culture was grown in a rotary shaker (12 h, 250 rpm, 37°C) until an optical density at 600 nm (OD_{600nm}) of 0.6 was achieved. Next, bacteria culture (2% v/v) was used to inoculate a bench fermentor containing 10 L of Terrific Broth media, glucose (0.8% w/v), ampicillin (100 mg/L), and antifoam B emulsion (4 mL). The fermentor was operated at 400 rpm and 36°C, with an air flow rate of 5 vvm. Expression was induced at $OD_{600nm} = 8$ by the addition of isopropyl β-D-1-thiogalactopyranoside (0.5 mM). Anti-foaming agent (anti-foam B) was added in small doses (1 mL) whenever necessary during bacterial growth. Finally, 4 h post-induction (approximate OD_{600nm} of 15), bacteria were harvested by centrifugation (10,000 rpm, 4°C) and stored at −80°C until further use.

EXTRACTION AND PURIFICATION OF RES-CBD

Bacterial pellets were thawed at 4°C and homogenized in a lysis buffer containing sodium phosphate (25 mM, pH 7.5), NaCl (150 mM), $MgCl_2$ (5 mM), and phenylmethanesulfonyl fluoride (1 mM). Next, the homogenized bacteria were sonicated (80% amplitude, 100% pulse time, 30 min; 500 V UIP1000hd industrial sonicator, Hielscher, Teltow, Germany) on ice and then centrifuged (10,000 rpm, 45 min, 4°C). The soluble fraction was removed, and the pellet containing the res-CBD in the form of inclusion bodies (IBs) was washed four times with IBs washing buffers (25:1 v/w buffer:pellet). Two washes were carried out using sodium phosphate (25 mM, pH 7.5), NaCl (150 mM) and Triton X-100 (0.8 wt%) buffer, followed by two additional washing steps using a sodium phosphate (25 mM, pH 7.5) and NaCl (150 mM) detergent-free buffer. The washed IBs containing 6H-17res-CBD were then dissolved in urea (6 M), sodium phosphate (25 mM, pH 7.5), and NaCl (150 mM), and the soluble fraction was collected for protein refolding. Refolding of the urea-dissolved protein was carried out via the drop-wise addition of refolding buffer (10:1 v/v of refolding buffer to urea-dissolved protein) containing sodium phosphate (25 mM, pH 8) and NaCl (150 mM). The refolded 6H-17res-CBD was then cleaved from its N-terminal histidine-tag fusion partner (His-tag) via recombinant Tobacco Etch Virus protease (rTEV), followed by Ni-NTA affinity chromatography purification, as has been previously described.[21] The His-tag-free res-CBD was collected from the column flow-through, dialyzed against deionized water, lyophilized, and stored at 4°C until further use. Soluble and pellet samples from each of the above res-CBD expression and purification steps were collected and analyzed by sodium dodecyl (lauryl) sulfate-polyacrylamide gel electrophoresis (SDS-PAGE).

CELLULOSE BINDING CAPACITY

The ability of refolded res-CBD to bind to a cellulose matrix was determined via a binding assay to microcrystalline cellulose (Avicel) as previously described.[27,30] Briefly, res-CBD solution (pH 8) was mixed with Avicel powder (1:300 w/w res-CBD: Avicel) and allowed to interact for 1 h at room temperature, after which centrifugation (14,000 rpm, 5 min, room temperature) was used to separate a supernatant (unbound res-CBD) and a pellet (Avicel bound to res-CBD). The crude mixture, the supernatant, and the pellet were analyzed by SDS-PAGE.

BINDING OF RES-CBD TO CNCs

The binding capacity of res-CBD to CNCs was tested by incubating mixtures of different mass ratios of res-CBD and CNCs ($\sim$2 wt%) for 1 h at room temperature in Tris buffer (pH 8, 4 mM), with gentle rotation of the sample. Mass ratios of 1:1, 1:5, 1:10, and 1:50 of res-CBD to CNCs were tested. After incubation, ultrafiltration was used to isolate unbound protein (Centricon membranes, 0.2-μm pore size, EMD Millipore, Billerica, MA), since unbound res-CBD (MW $\approx$ 53 KDa) passes through the membrane, whereas the CNCs used in this work did not. The different mass ratio mixtures were centrifuged (14,000 rpm, 5,000 g) long enough such that $\sim$50% of the liquid permeated the membrane. Permeate and retentate fractions were collected and analyzed by SDS-PAGE to determine conditions for optimal binding. In addition, pure res-CBD was used as a control in order to establish non-specific interaction between the proteins and the membrane, while pure CNCs were used in order to establish that CNCs do not pass through the membrane (data not shown). Equal amounts of protein (3.5 μg, assuming equal protein concentrations in each fraction) from the crude mixture, retentate, and permeate of each of the tested mass ratios were loaded and separated on the acrylamide gel (12.5%), and compared to a protein ladder (7 μL, MW range 250–10 KDa) and to a sample of pure res-CBD (3.5 μg).

CNC AND RES-CBD-CNC CHARACTERIZATION

The physicochemical properties of the pure CNCs and res-CBD-CNCs are presented in *Table 1*.

FOURIER TRANSFORM INFRARED SPECTROSCOPY (FTIR)

FTIR spectra of freeze-dried samples were obtained using a Nicolet 6700 (Thermo Fisher Scientific Inc., Waltham, MA). A mortar and pestle was used to combine 2 mg of sample with 98 mg of KBr, which was then pressed into a pellet for FTIR spectroscopy.

PREPARATION OF RES-CBD-CNC FILMS

Freeze-dried res-CBD was dissolved in CNC suspensions at a 1:10 w/w res-CBD:CNC ratio. A series of films were cast from res-CBD-CNC suspensions (2.5 wt% CNCs, 0.25 wt% res-CBD, 20 mL suspension volume per film), with dry film glycerol loadings of 0 wt%, 0.5 wt%, 2.5 wt%, 5 wt%, and 25 wt%. Prior to film casting, the mixtures were gently rotated at room temperature for 1 h to allow time for binding. The films were prepared by solution casting onto Sigmacote-treated glass substrates (7 cm $\times$ 5 cm), and were dried for several days under ambient conditions until constant weight was achieved. Finally, the dried films were detached and cut using a scalpel to produce rectangular strips (4-cm length $\times$ 5-mm width $\times$ $\sim$40-μm thickness). CNC films were prepared in the same manner as described for the res-CBD-CNC films, as were control films prepared from mixtures of CNCs and *D. melanogaster* 17 repeat exon 1 proresilin (CNC/res), and CNCs and *C. cellulovorans* CBDs (CBD-CNC), at 0 wt% and 5 wt% glycerol.

Table 1. General Characteristics of CNCs and res-CBD-CNCs

	UNBOUND CNCs	RES-CBD-CNCs
%S by conductometric titration	1.04 (0.03)[a]	[b]
Zeta-potential (mV)	−56.29 (1.41)	−42.2 (1.6)
Electrophoretic mobility (m^2/Vs)	−4.40 (0.11)	−3.3 (0.1)
Mean particle size by NanoSight (nm)	105 (11)	143 (10)

[a]Standard deviations are presented in parentheses.

[b]The sulfur content of the CNCs was assumed to be unchanged by binding with res-CBD; however the %S was not tested after binding.

AFM

Three different AFM instruments were used:

(1) Dilute samples for AFM were deposited onto Piranha-cleaned silicon wafers by spin-coating according to the following sequence: (i) 0.1 wt% polyethylene imine, (ii) deionized water, and (iii) 0.01 wt% CNCs or res-CBD-CNCs. The samples were imaged using a JPK Instruments (Berlin, Germany) NanoWizard3 AFM in tapping mode.
(2) AFM images of film surfaces prepared using the same spin-coating sequence described in (1) but concentrated suspensions (2 wt% CNCs or res-CBD-CNCs) were used and images were obtained in PeakForce™ mode using a BioScope Catalyst AFM (Bruker, Billerica, MA). These films were also used for contact angle measurements.
(3) The thicknesses of the films used for contact angle measurements were determined using scratch height tests in contact mode with an MFP-3D AFM (Asylum Research, Oxford Instruments, Austin, TX).

CONTACT ANGLE

Films for contact angle measurements were prepared using the same spin-coating sequence described above in (2). The films were heated overnight at 60°C prior to contact angle measurement to avoid redispersion of the CNCs when in contact with water. Advancing water contact angles were measured using a KSV (Helsinki, Finland) Theta Optical Tensiometer. A minimum of 10 measurements were obtained per sample, and the results presented are an average.

SCANNING ELECTRON MICROSCOPY (SEM)

Films were sputter-coated with gold (12 mA, 6 min) using an S150 sputter coater (Edwards), and imaged using the MagellanTM 400L.

POLARIZED LIGHT MICROSCOPY

An LC-PolScope™ system (Cambridge Research and Instruments, Woburn, MA) mounted onto a Nikon Eclipse 80i was used to study orientation within the CNC films. The LC-PolScope image-processing system extends the capability of traditional polarized optical microscopy since it can quantify retardance/birefringence, and indicate molecular orientation, which is proportional to the angular shift in polarized light that occurs as it passes through a birefringent sample. In addition, a Nikon Eclipse LV100N POL microscope with a 530-nm waveplate inserted in the light path between sample and analyzer was used to explore the nature of the film's orientation.

INSTRON TESTING

Tensile tests of the CNC-based films were performed using an Instron (Instron 3345 Tester, Instron, Norwood, MA) equipped with a 100-N load cell and using a crosshead speed of 1 mm/min. The width and length of the film strips between the Instron clamps were measured using a digital caliper (0–150 mm), and an average thickness was obtained by measuring 5 random positions along the film length using a Mitutoyo Digimatic Indicator (Type ID-S112MB, Mitutoyo Manufacturing Co. Ltd., Kawasaki, Japan).

DYNAMIC MECHANICAL ANALYSIS (DMA)

DMA measurements of the films were performed using a Q800 DMA (TA Instruments, New Castle, DE) in a strain-controlled mode, at frequencies of 0.1, 1, 10, 20, and 100 Hz, and a temperature of 25°C.

NANOINDENTATION

Nanoindentation was performed using a Micro Materials (Wrexham, UK) NanoTest™ system on free-standing film strips ($\sim$40-μm thick) that were adhered onto glass slides with double-sided tape. The films should ideally be adhered directly to the solid substrate in order to avoid any influence from the adhesive; however, it is challenging to prepare reasonably thick CNC and res-CBD-CNC films adhered onto a substrate using the same conditions because of wettability differences. Thus, the nanoindentation results presented in this work are valid in terms of sample comparison since they were prepared identically, but may not be entirely accurate due to contributions from the double-sided tape. Nanoindentation was performed in a load controlled mode with a Berkovich diamond indenter calibrated for load, displacement, frame compliance, and indenter shape according to ISO14577-4 procedure. The area function for the indenter was determined by indentations of 0.5–500 mN into a fused silica reference sample. For nanoindentation of the films, the peak load was 10 mN, and 30 indentations were performed for each film. This load was chosen to minimize the influence of substrate on the data while ensuring that the indentation contact depth was less than 1/10th of the film thickness, so that a film-only (load-invariant) hardness could be measured in combination with film-dominated elastic modulus. Nanoindentation was performed at room temperature on films that were equilibrated under ambient conditions for several days.

ERROR ANALYSIS

Standard deviations (SDs) are provided within brackets in *Table 1*. In all other instances, variation in the data is given by a standard error calculated using the Student's *t*-test (*Equation 1*), where n is the number of independent measurements, and $t_{95\%}$ is the t-value at 95% confidence and n-*1* degrees of freedom:

$$Standard\ error\ (\pm) = t_{95\%} \times SD/n^{0.5} \qquad (Equation\ 1)$$

Results and Discussion

EXPRESSION AND ISOLATION OF RES-CBD

The chimeric gene, consisting of 17 elastic repeats from the exon 1 of the *D. melanogaster resilin* gene, which was C-terminal fused to a *C. cellulovorans CBD* gene, was successfully cloned (gene sequence is provided in *Fig. S1*; Supplementary data are available online at www.liebertpub.com/ind), expressed in *E. coli*, and purified from the inclusion bodies of the bacteria.[27,30] *Figure 1* presents the SDS-PAGE analysis of the total bacteria prior to purification, which showed an intense band at $\sim$55 kDa corresponding to 6H-17res-CBD (*Fig. 1A*). SDS-PAGE analysis

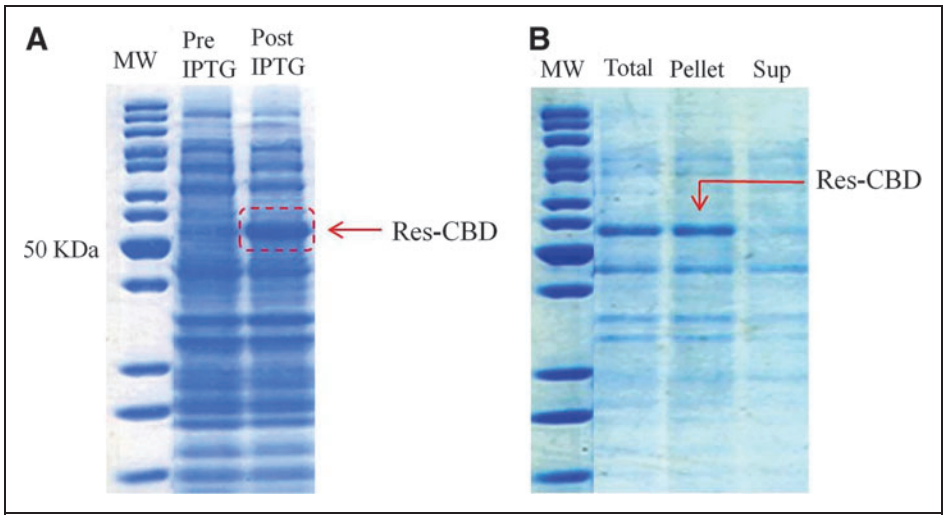

Fig. 1. Expression and purification of 6H-17res-CBD. **(A)** SDS-PAGE analysis of protein expression in BL-21 (DE3) bacteria; **(B)** SDS-PAGE analysis of supernatant and pellet fraction post sonication of 6H-17res-CBD-expressing bacteria, showing that the protein is concentrated within the inclusion bodies.

of the supernatant and pellet fractions of the sonicated bacteria revealed that the variant was expressed within the inclusion bodies and localized in the pellet fraction (*Fig. 1B*). SDS-PAGE analysis indicated only minor protein loss throughout the isolation of a highly purified res-CBD post-refolding (*Fig. 2A*). Gene cloning, expression, and purification, including Western blot analysis was as in Rivkin et al.[28] Furthermore, the proper refolding of the protein was reflected by its ability to bind to microcrystalline cellulose powder (Avicel), as was demonstrated by SDS-PAGE of the unbound and bound fractions isolated by centrifugation after incubation of the protein/cellulose mixture (*Fig. 2B*).

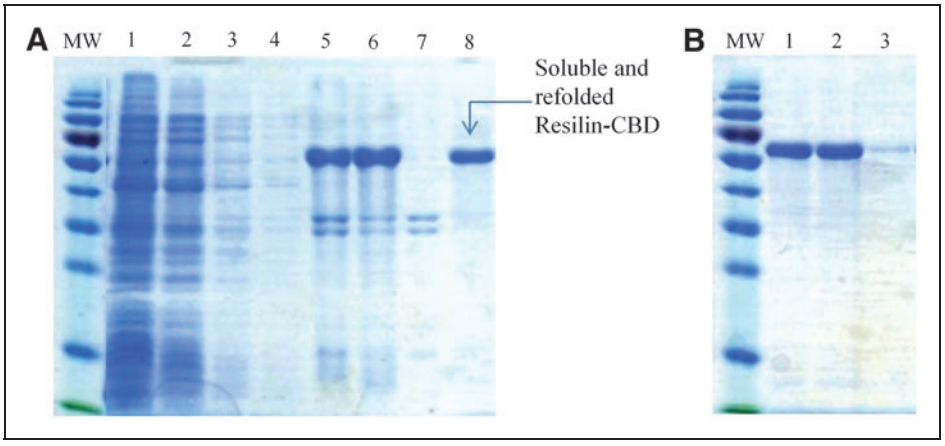

Fig. 2. Res-CBD purification and refolding using IBs washing, solubilizing, and refolding techniques. **(A)** SDS-PAGE analysis of purification and refolding steps: Supernatants from IBs washing steps (*lanes 1–4*); total, supernatant, and pellet of urea dissolved IBs (*lanes 5–7*, respectively); and supernatant of urea dissolved IBs post-refolding (*lane 8*). **(B)** SDS-PAGE analysis of Avicel binding to refolded res-CBD: total proteins, cellulose bound res-CBD, and unbound res-CBD (*lanes 1–3*, respectively).

BINDING OF RES-CBD TO CNCs

The optimal binding of res-CBD to CNCs under the conditions used in this work was observed at a mass ratio of 1:5 res-CBD to CNCs (see SDS-PAGE in *Fig. 3*). Aside from the mass ratio of res-CBD to CNCs, all other conditions (pH, buffer concentration) were kept constant in order to minimize potential ionic strength effects on the observed binding. It was found by SDS-PAGE analysis that a mass ratio of 1:1 res CBD to CNCs overloaded the CNCs with res-CBD, as a significant band from unbound protein was seen in the permeate, whereas the res-CBD was fully bound at 1:5, 1:10, and 1:50 mass ratios. Therefore, the mass ratio of 1:5 represents the condition that fully binds the most res-CBD, although further fine tuning between the 1:1 and 1:5 mass ratios may be possible. Finally, although the 1:5 mass ratio was determined to be optimal, the films in this work were prepared at the 1:10 binding condition in order to be consistent with recent work that studied epoxy-based res-CBD-CNC nanocomposites and found significant improvements in mechanical properties at this mass ratio.[29]

The res-CBD content (1:10 res-CBD to CNCs) was expected to change the chemical signature as well as the physical properties of the CNCs. Indeed, infrared spectroscopy showed new absorption bands in res-CBD-CNCs, which were related to the protein amino acids (*Fig. 4*).[6,30] Absorption bands at 1,500/cm (indicating the presence of aromatic amino acids) and 1,220/cm (indicating C-N stretch) in res-CBD-CNCs are absent in the neat CNC spectrum, and the band at 1,650/cm is strengthened relative to the neat CNC film due to N-H bending. In addition, the appearance of the res-CBD-CNCs is mostly unchanged by res-CBD binding, as seen by AFM (*Fig. 5*), although some longitudinal aggregates were visible. It is, however, difficult to make direct comparisons regarding the state of dispersion of the samples from the AFM images since the surface coverage of the films were different. This was likely due to differences in sample wettabilities, which are addressed below. Zeta-potential and NanoSight measurements indicated that the res-CBD-CNCs remained colloidally stable (*Table 1*). In general, we concluded that the appearance, aqueous dispersibility, and colloidal stability of the CNCs were not detrimentally impacted by the binding of res-CBD.

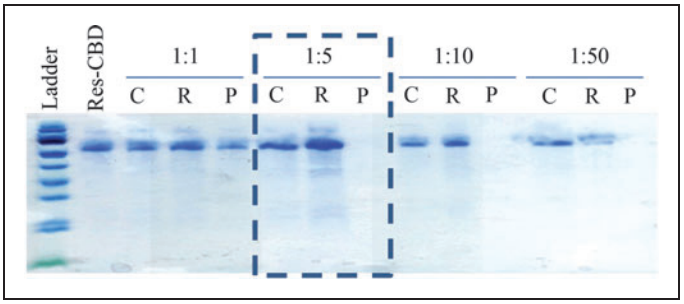

Fig. 3. SDS-PAGE showing binding of res-CBD to cellulose nanocrystals at different mass ratios of res-CBD to cellulose nanocrystals. From left to right: protein ladder, res-CBD control, and crude (C), retentate (R), and permeate (P) samples from 1:1, 1:5, 1:10, and 1:50 mass ratios of res-CBD to CNCs.

PREPARATION OF RES-CBD-CNC FILMS

Res-CBD-CNC films were prepared by spreading the aqueous suspensions onto flat glass plates pretreated with a hydrophobic commercial coating, followed by water evaporation under ambient conditions. The transparent coating solution (Sigmacote) is composed of chlorinated organopolysiloxane in heptane and leaves a neutral, hydrophobic coating on glass substrates. The pretreatment was necessary since res-CBD-CNC films adhered so strongly to uncoated glass that they could not be removed. Furthermore, film casting provided the first indication of differences in the wettabilities of CNCs and res-CBD-CNCs, since neat CNC films could be peeled off of untreated glass and res-CBD-CNCs spread more easily on the coated glass. The water content of the films was not controlled, and the glycerol-containing films were more likely hygroscopic. Both CNC and res-CBD-CNC films appeared transparent (with and without glycerol); however, the res-CBD-CNC films were less brittle and easier to handle than neat CNC films (*Fig. 6*). In addition, *Fig. 6* shows that bending of the CNC films leads to cracking and plastic deformation, whereas the res-CBD-CNC films are easily deformed and relax back to their original shape once released.

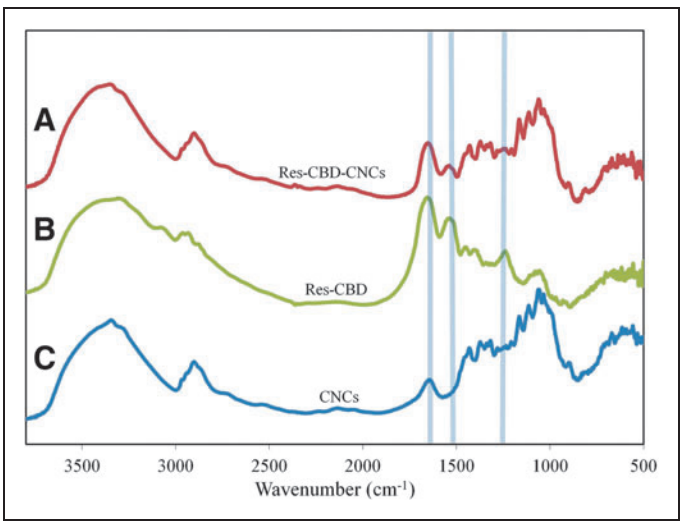

Fig. 4. FTIR spectroscopy of **(A)** res-CBD-CNCs; **(B)** res-CBD; and **(C)** neat CNCs.

Glycerol was added to the films in order to determine whether the mechanical performance of the res-CBD-CNC films could be improved by the presence of a high-boiling/water-compatible liquid. We note that CNC films loaded with glycerol alone were also less brittle and easier to handle, similar to the res-CBD-CNC film depicted in *Fig. 6*. It was hypothesized that glycerol-solvated res-CBD-CNCs would confer improved elastic properties in comparison to films without glycerol, since the elastic response of hydrogels based on resilin/resilin-like polymers has been critically linked to its state of hydration/solvation.[32] Weis-Fogh first commented on the importance of water in the elasticity of natural resilin from locust cuticles; dehydration of the rubbery material made the samples hard and brittle, but the elasticity could be recovered by reswelling in water or other polar solvents, such as glycerol.[7] Furthermore, although not explicitly studied in the current work, we anticipate that the presence of glycerol in res-CBD-CNC systems may extend the potential usage of these materials to higher temperature/dehydrated conditions, in which the water in the system is driven off but the glycerol remains (glycerol boiling point = 290°C).

SURFACE AND MORPHOLOGICAL FILM CHARACTERIZATION

Advancing water contact angle measurements were conducted to quantify the increase in hydrophobicity of res-CBD-CNC films compared to neat CNC films, which had been qualitatively observed during film preparation (i.e., res-CBD-CNCs better wet the hydrophobically treated glass surfaces). *Figure 7A* compares the advancing water contact angles of the films as a function of glycerol loading. Indeed, the res-CBD-CNC films were significantly more hydrophobic than the neat CNC films, with contact angles in the range of 70–80°, compared to 35–40° for the CNC films. However, the average contact angle of both the CNC and the res-CBD-CNC films was largely unchanged by the addition of glycerol (within experimental error), indicating that the hydrophilic additive preferentially resides within the film bulk and is not present at the film surface.

The increase in contact angle for the res-CBD-CNC films is attributed to hydrophobic protein residues partitioning at the air-film interface. Family III CBDs have planar hydrophobic binding sites comprised of aromatic amino acids, and binding to crystalline cellulose is thought to occur at the hydrophobic crystal edge.[33–35] The increase in contact angle observed for the res-CBD-CNC films may thus be related to CBD moieties at the film surface.[30] The contact angle increase may also be attributed to resilin; Dutta et al. reported water contact angles of 63° for smooth, thin films of resilin spin-coated onto silicon wafers (resilin from *D. melanogaster* gene, exon 1) and related the moderately high contact angle to the morphology adopted by resilin adsorbed onto a hydrophilic surface.[36] *Figure 7B* proposes a film structure to explain the increased contact angle, where the res-CBD-CNC film is considered as alternating hydrophilic/hydrophobic phases, with a relatively hydrophobic protein phase located at the film surface. Regardless of the precise source of the increased hydrophobicity, the contact angle results presented here are consistent with the recent work of

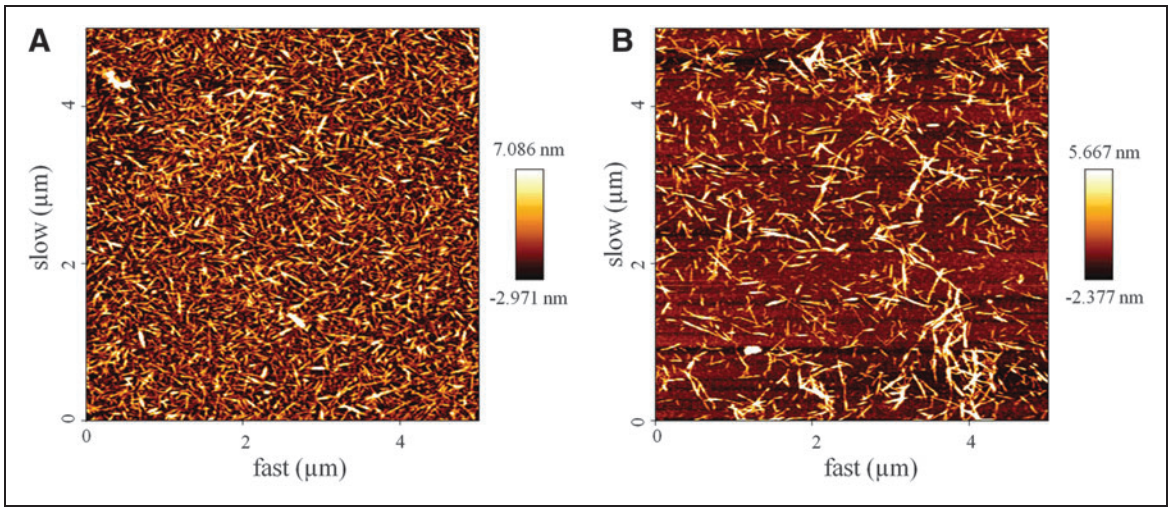

Fig. 5. AFM height images of **(A)** pure CNCs and **(B)** CNCs bound to res-CBD at a 1:10 mass ratio of res-CBD to CNCs. Scans are of 5 μm × 5 μm square areas.

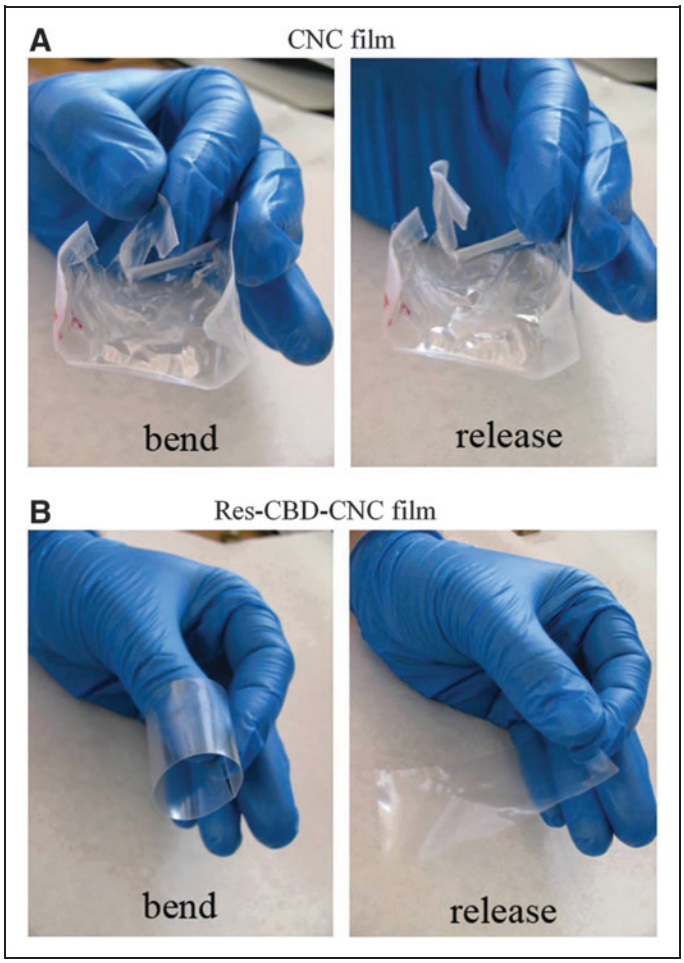

Fig. 6. Bending of **(A)** CNC and **(B)** res-CBD-CNC films that were prepared by casting onto pretreated glass under ambient conditions.

Verker et al., which found that unlike neat CNCs, res-CBD-CNCs were readily dispersed into the epoxy matrix, implying good adhesion between the res-CBD-CNCs and the matrix.[29]

In addition, the contact angle differences could not be explained by any surface morphological features or variations in roughness. AFM images (*Fig. S2*) showed unremarkable film surfaces, with radial particle alignment from the spin-coating deposition method. Finally, two types of CNC films at 0 wt% glycerol were measured—a sodium-form CNC film cast from a pH 8 suspension, and an acid-form CNC suspension cast from a pH 3 suspension (*Fig. 7A*). The contact angle of the acid-form film exceeded that of the Na-form film by approximately 10° due to the improved redispersibility/water uptake of Na-form CNC films; Beck et al. have shown that films cast from Na-form CNCs readily redisperse in water, even when fully dried, whereas H-form CNCs only redisperse when the water content of the films is greater than 4 wt%.[37] We note that res-CBD-CNC films that have not been heat-treated fully redisperse in water with brief sonication, but that the redispersion of heated films was not explored.

SEM of film cross-sections generated by the fracture of flash-frozen films was used to investigate film morphology and the role of glycerol in the films (*Fig. 8*). No morphological differences stand out between the res-CBD-CNC films and the CNC films, with or without added glycerol. The films without glycerol show the typical internal layered structure of CNC films, however glycerol seems to be coating/lubricating the CNC layers in the images of the CNC film with 25 wt% glycerol and the res-CBD-CNC films with 5 wt% and 25 wt% glycerol.[38] These images substantiate the view presented above that glycerol is principally concentrated within the film bulk, and also raises the question as to whether glycerol-coated CNCs show reduced cohesion compared to uncoated CNCs. Similar to paper sheets, the strength of CNC films and nanocomposites is often attributed to hydrogen bonding between CNCs (although in nanocomposites adhesive interactions are also important to the

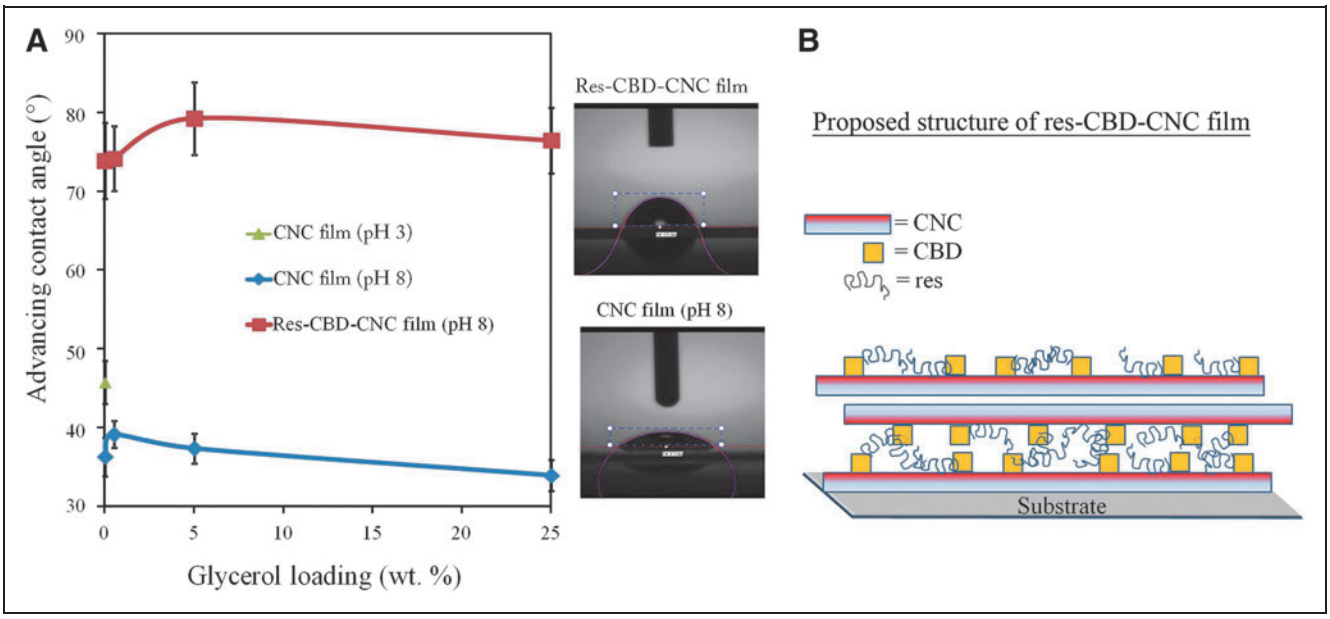

Fig. 7. (A) Advancing water contact angles of neat CNC and res-CBD-CNC films with varying glycerol contents from 0–25 wt%. The res-CBD-CNC films were cast from pH 8 suspensions, and two CNC films were prepared—one cast from pH 8 and the other from pH 3; **(B)** schematic representation of res-CBD-CNC film structure, with protein domains at the surface-air interface.

overall strength), and it is unclear whether glycerol disrupts H-bonding between CNCs to a detrimental effect. The mechanical properties of the films are presented below and look more closely at the role of glycerol in these films.

POLARIZED OPTICAL MICROSCOPY

The rod-like shape of CNCs leads to entropically driven particle alignment in suspension and films.[39] Above a critical concentration, CNC suspensions undergo phase separation into an upper isotropic phase and lower chiral nematic phase. The lower chiral nematic phase is characterized by pseudo-layers of aligned CNCs where the average orientation of each layer is offset from the layer above and below in such a way that it rotates helically through the pseudo-layers.[40–42] The chiral nematic orientation in suspension can be 'frozen' into solid films by the slow evaporation of water, which shifts the CNC organization from isotropic to ordered as the concentration increases.[39,43–45] In addition to chiral nematic films, nematic CNC films with unidirectional particle alignment have also been observed.[46] Nematic ordering in CNC suspensions implies an environment that prevents the transmission of chirality and has been ascribed to conditions that obscure the hypothesized right-handed threaded structure and/or surface charge distribution of CNCs. Experimentally, CNC suspensions at low ionic strength, where the electrostatic double layer is large, organize in a nematic fashion.[46,47]

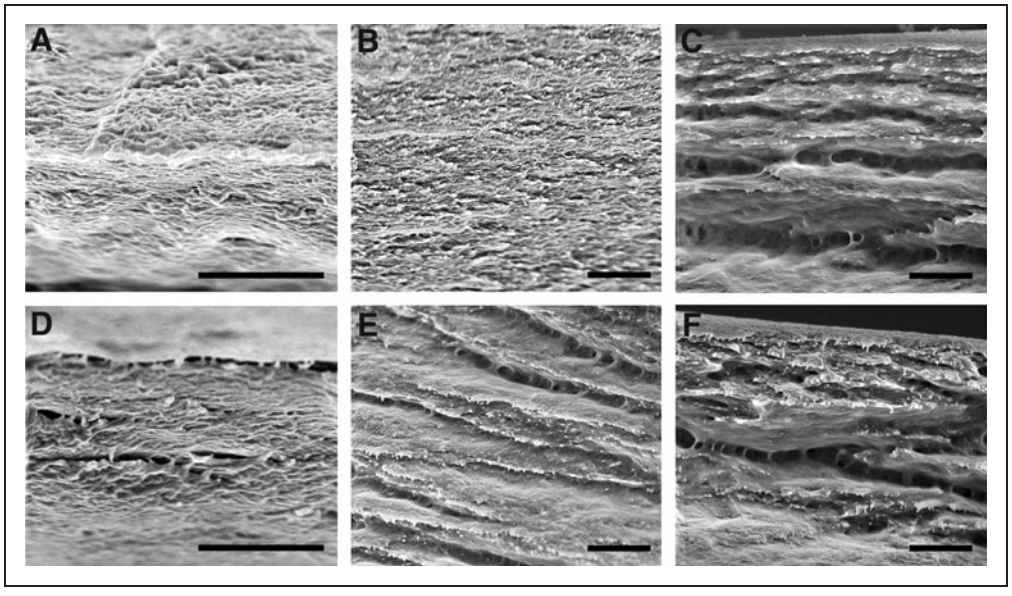

Fig. 8. SEM images of cross-sectional areas of (**A–C**) CNC films at 0 wt%, 5 wt%, and 25 wt% glycerol, respectively; and (**D–F**) res-CBD-CNC films at 0 wt%, 5 wt%, and 25 wt% glycerol, respectively. Scale bars = 500 nm.

The alignment of CNCs in the free-standing films prepared here was explored using polarized optical microscopy (POM) coupled with an image-processing module that is able to confer the direction of sample alignment.[48] *Figures 9* and *10* present the POM images of

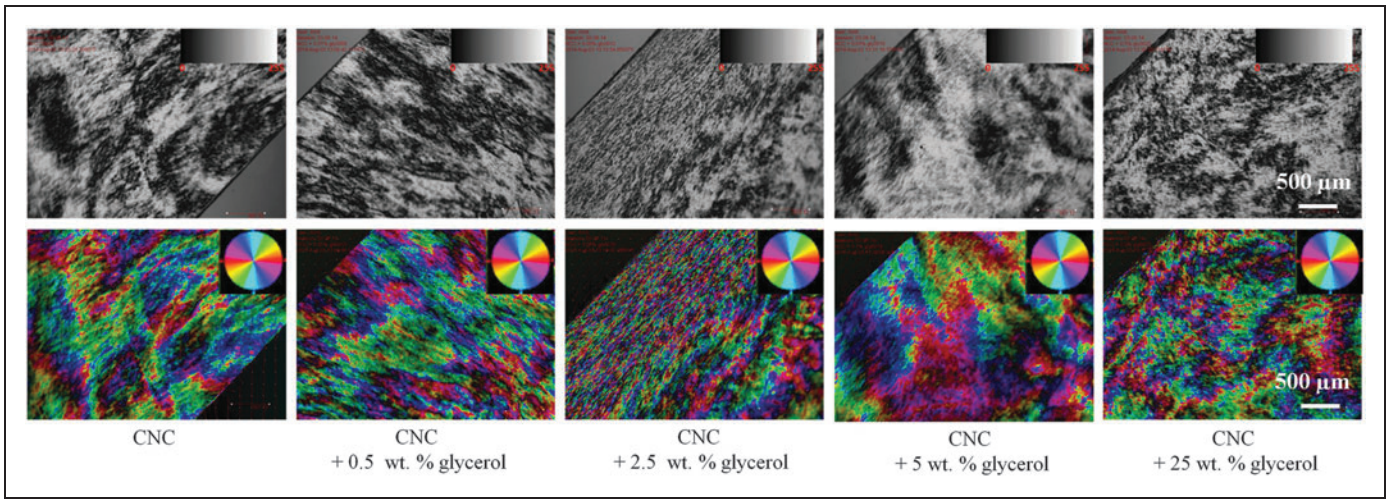

Fig. 9. Top panel presents POM images of CNC films with increasing loadings of glycerol from left to right, and bottom panel shows the result of the LC-PolScope birefringence analysis performed on the POM images. CNC films at all glycerol loadings have similar multi-domain orientation. The color wheel in the upper-right hand corner of the processed images corresponds to the orientation of the slow optical axis.

CNC and res-CBD-CNC films, respectively, with increasing glycerol contents from left to right. The top panels show traditional POM images, with bright regions indicative of alignment and dark regions indicative of disorder and/or order in the viewing plane, and the bottom panels show the processed birefringence images in which the orientation (azimuth) of the slow optical axis is shown. The CNC films presented in *Fig. 9* (with and without added glycerol) are birefringent and show the typical fragmented, multi-domain order that is characteristic of chiral nematic CNC films prepared by water evaporation.[38] In contrast, the res-CBD-CNC films (*Fig. 10*) appear uniformly birefringent, and the polarized microscopy image-processing technique interprets long-range nematic order similar to that observed when CNC suspensions are sheared (*Fig. S3*).[49] *Figure 11* shows the corresponding images for CBD-CNC and res/CNC films; the CBD-CNC films have the same appearance as the res-CBD-CNC films, whereas the patch-like, interrupted birefringence of the res/CNC film resembles the neat CNC film.

These observations suggest that the CBD, and not resilin, is responsible for the long-range, unidirectional alignment observed in the res-CBD-CNC films. To the best of our knowledge, this is the first report of alignment induced in CNC films

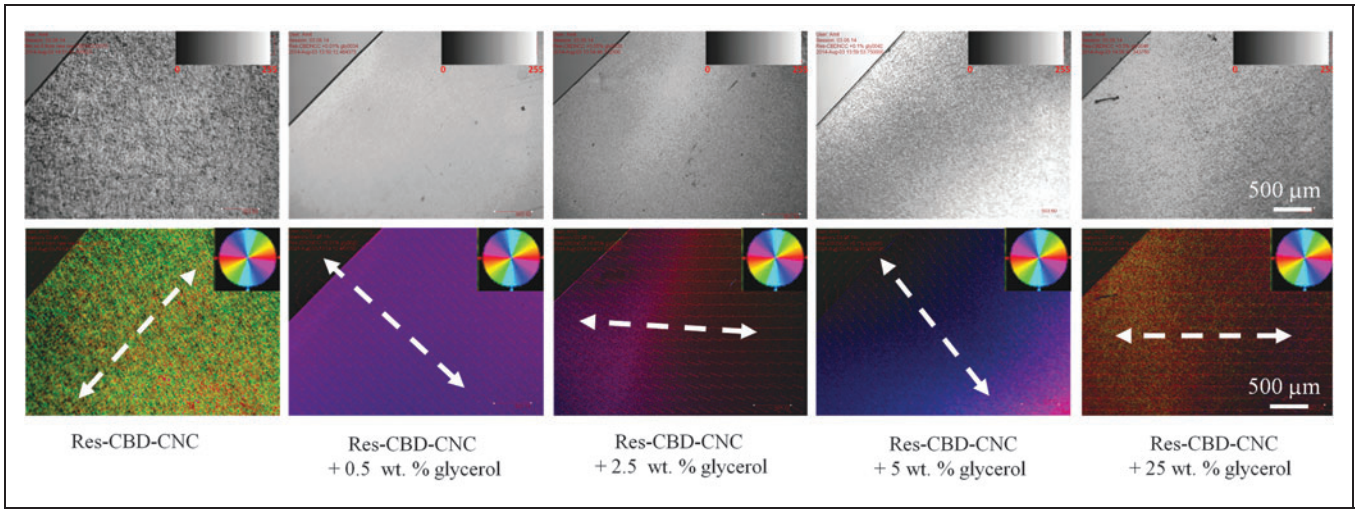

Fig. 10. Top panel presents POM images of res-CBD-CNC films with increasing loadings of glycerol from left to right, and bottom panel shows the result of the LC-PolScope birefringence analysis performed on the POM images. Res-CBD-CNC films at all glycerol loadings are characterized by long-range unidirectional orientation, with white arrows indicating the average direction of the slow optical axis. The color wheel in the upper-right hand corner of the processed images corresponds to the orientation of the slow optical axis.

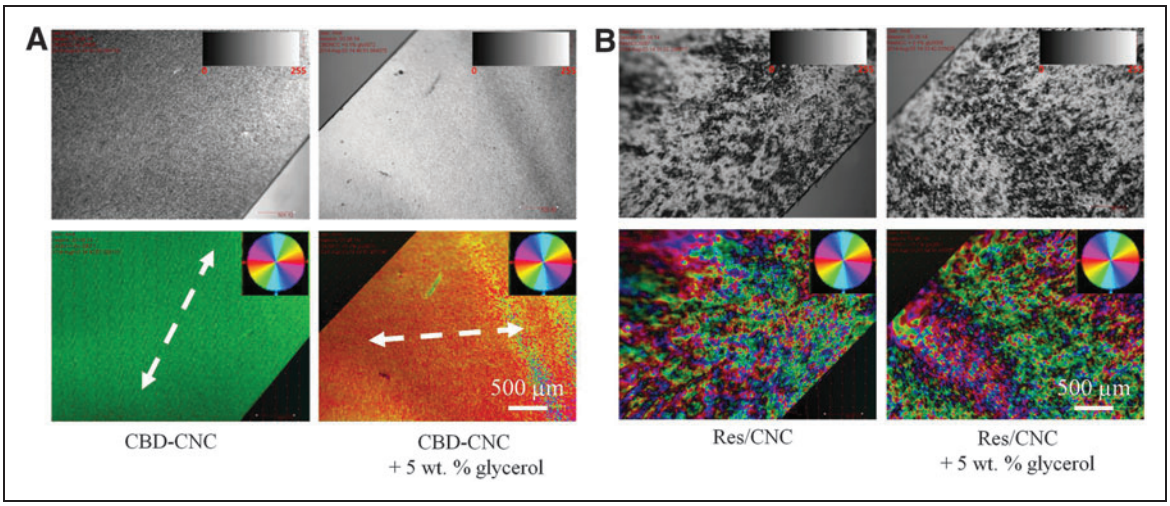

Fig. 11. Top panels show the POM images and bottom panels show the LC-PolScope birefringence analysis; **(A)** POM and associated processed images for CBD-CNC films and **(B)** POM and associated processed images for res/CNC films. CBD-CNC films show uniaxial long-range order, whereas the res/CNC films appear more fragmented. The color wheel in the upper-right hand corner of the processed images corresponds to the orientation of the slow optical axis, with the white arrows in Fig. 11A indicating average orientation.

prepared by solvent evaporation in the absence of external forces and apparently due to CBD binding. Furthermore, the CNC and res/CNC films were chiral nematic (i.e., fingerprint pattern seen in POM images), whereas the order in the CBD-CNC films was nematic (*Fig. S4*). It is not uncommon for chiral nematic phases to be observed in systems prepared from mixtures of hydrophilic (neutral or anionic) polymer and CNCs. Assuming that a screw-like shape/surface feature is responsible for the chiral nematic ordering of CNCs, it is possible that CBD-binding somehow obscures this effect, perhaps by binding within the groove of a thread or due to the flexible nature of the CBD. The binding of Family III CBDs occurs via the interaction of the planar strip of aromatic residues with the hydrophobic edge of a cellulose chain, and is stabilized by polar amino acid residues that anchor the CBD to two other cellulose chains.[34] Possibly, the CBD-induced alignment in the CNCs occurs because the CBD is able to bridge two cellulose nanocrystals—a theory that is supported by apparent aggregates in the AFM images of dilute res-CBD-CNCs (*Fig. 5*). It is also possible that hydrophobic/hydrophilic phase-separation interactions in the res-CBD-CNC and CBD-CNC systems play a role in the observed alignment (see *Fig. 7B*).

MECHANICAL CHARACTERIZATION

We were interested in understanding the mechanical properties of films made by combining one of nature's strongest materials, CNCs, with the polymeric precursor of one of nature's most elastic materials, resilin; in this case, specifically exon 1 resilin bound to a CBD moiety. The mechanical tests used to evaluate the effect of res-CBD binding on the material properties of CNC films included Instron testing, DMA, and nanoindentation. The resilin loading used in this work was fixed at 10 wt% of the dry CNC weight (with an initial CNC concentration of 2.5 wt%) and the films contained different glycerol loadings, ranging from 0 wt% to 25 wt% of the dry film weight. The Instron and DMA tests were in tensile mode and probed the *x-y* in-plane structure of the films, whereas the nanoindentation measured the response to compression in the *z*-direction.

Instron testing. Figure 12 shows the Instron tensile testing results for CBD-CNC, res-CBD-CNC, and neat CNC films. Overall, the results highlight that the mechanical behavior of the films is similar, and large error intervals are attributed to the difficulty associated with the tensile testing of relatively brittle CNC-based films. In *Fig. 12*, glycerol in CNC films is shown to reduce the average modulus and increase the average elongation at break, without sacrificing average tensile strength or average toughness, for glycerol contents below 5 wt%. However, the addition of 25 wt% glycerol led to a significant reduction in the average tensile strength and toughness of the CNC films. The mechanical properties of CNC films with added glycerol were consistent with the addition of a softening component, and practically, this meant that CNC films containing glycerol were easier to handle since they were less brittle. The decrease in modulus with added glycerol implies that glycerol indeed disrupts CNC cohesive interactions; i.e., that the adhesion between CNCs and glycerol is weaker than CNC cohesive interactions.

In comparison to the other films studied, res-CBD-CNC films loaded with glycerol had higher average moduli and tensile stress and strain values at break, resulting in tougher films on average (*Fig. 12B*). Furthermore, the tensile strength of the res-CBD-CNC films was the only parameter that was reduced when the glycerol content was increased to 25 wt% (*Fig. 12C*). For the CBD-CNC films without resilin, the average modulus, tensile strength and strain, and toughness were similar at both of the glycerol contents that were studied—0 wt% and 5 wt%—and were similar to the corresponding CNC film results; however, at 5 wt% glycerol, the res-CBD-CNC film outperformed the CBD-

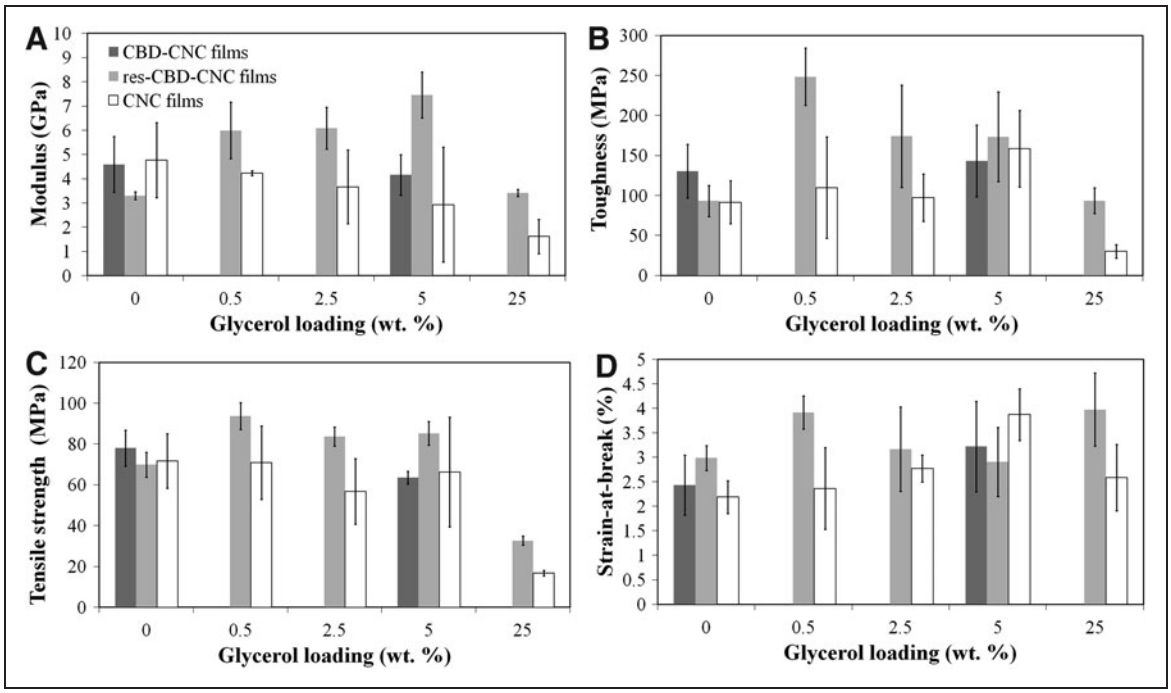

Fig. 12. Results from Instron tensile testing of films; **(A)** modulus; **(B)** toughness; **(C)** tensile strength; and **(D)** strain-at-break. The figure legend is indicated in 12A; dark gray bars correspond to CBD-CNC films, white bars to CNC films, and gray bars to res-CBD-CNC films. The modulus values were calculated from the slope of the linear region of stress-strain curves, toughness is the area under the stress-strain curve, and tensile strength and strain-at-break are the maximum stress and strain that the films were able to withstand before break. Data points are an average from the measurement of 3–8 films, and error bars are calculated using a Student's t-test with 95% confidence.

CNC film in average modulus and tensile strength, suggesting that part of the improvement in mechanical performance in the res-CBD-CNC films with added glycerol can be attributed to resilin.

The improvement in the mechanical properties of the res-CBD-CNC films relative to CNC films may be related to improved interactions between CNCs due to the presence of res-CBD; resilin's polar residues may contribute to hydrogen bonding and/or reinforcing electrostatic interactions with CNCs, and CBD-induced CNC alignment may also contribute a strengthening effect. Furthermore, the improvement in mechanical properties with added glycerol for res-CBD-CNC films compared to CNC films suggests that glycerol has a different role to play in the two kinds of films; as mentioned above, the CNC film is softened by the addition of glycerol, but res-CBD-CNC films are strengthened by glycerol. This may indicate that

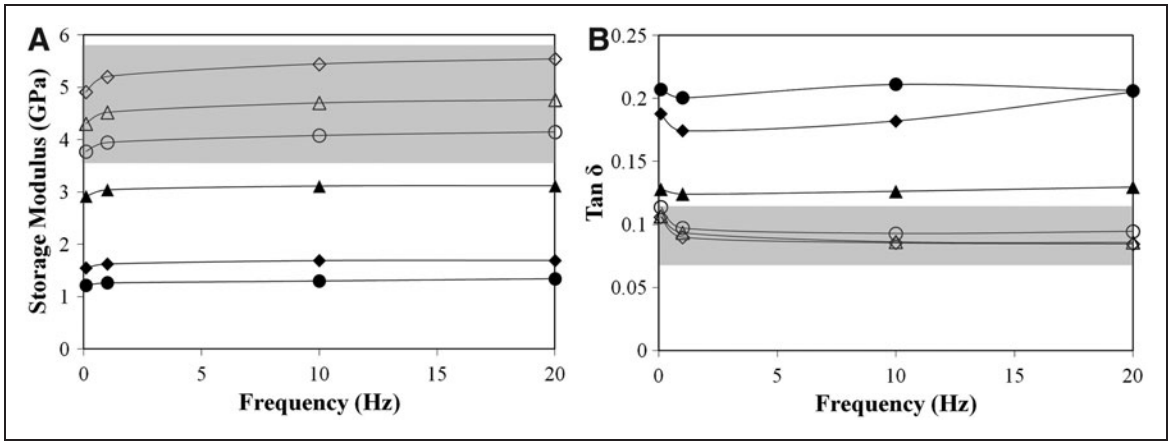

Fig. 13. DMA plots of **(A)** average shear modulus and **(B)** average tan δ of CNC and res-CBD-CNC films at different glycerol loadings. Shading is used to differentiate the res-CBD-CNC curves from the CNC curves, with res-CBD-CNC data highlighted in gray. Open symbols are for the res-CBD-CNC films, closed symbols for the CNC films; diamonds for 0 wt% glycerol, triangles for 0.5 wt% glycerol, and diamonds for 5 wt% glycerol. Each data point is an average of 3–6 samples, and lines between points are intended as visual guides.

when res-CBD is solvated by glycerol it is able to extend and bridge CNCs (e.g., via polymer entanglements and/or hydrogen bonding/electrostatic interactions with CNCs), leading to an average improvement in tensile properties. The results shown in *Fig. 12* suggest that a glycerol loading of 0.5 wt% for the res-CBD-CNC films gives the best mechanical performance in terms of toughness, surpassing the glycerol-free res-CBD-CNC film and neat CNC film by 150%.

DMA. DMA was used to characterize further the viscoelastic properties of the films as a function of frequency in strain-controlled mode (i.e., strain was fixed at 0.2%, a value that was predetermined to lie within the elastic response of the films). The general trends in storage modulus and tan δ for a series of films is presented in *Fig.13*; the average storage modulus values of the res-CBD-CNC films exceeded the CNC film values (*Fig. 13A*), and the average tan δ values of the res-CBD-CNC films were clustered below the CNC film tan δ values (*Fig. 13B*). However no trend in regards to glycerol loading was observed. The results in *Fig. 13* suggest that the res-CBD-CNC films on average have higher storage moduli (i.e., they are stiffer) and dissipate less of the mechanical energy during oscillation extensions applied within elastic region of the films (i.e., they are less viscous/more elastic). Thus, when strained to the same extent, on average res-CBD-CNC films uptake more mechanical energy and revert to their unstrained state more elastically in comparison to CNC films. The improved average storage moduli of the res-CBD-CNC films relative to the CNC films (at all glycerol loadings) mirrors the Instron results, where it was suggested that res-CBD enhances the tensile properties of the films through hydrogen bonding/electrostatic bridging interactions and by CBD-induced alignment. Furthermore, the increased elasticity for the res-CBD films seen in the tan δ DMA plot (*Fig. 13B*) is attributed to the presence of res-CBD, perhaps suggesting that uncrosslinked resilin is able to impart some elasticity to the CNC films.

Nanoindentation. Nanoindentation measurements were expected to be less sensitive to micro/bulk film defects introduced during sample preparation and would therefore give more reproducible and accurate results. Indeed, the error bars in *Fig. 14* indicate more precise measurements compared to the other mechanical methods used in this work. *Figure 14* plots the relevant parameters obtained by nanoindentation: hardness, reduced elastic modulus, elastic recovery parameter, and plasticity index. Hardness is a measure of the resistance of the films to penetration, and the reduced elastic modulus (E^*) is related to the modulus of the films (E) according to *Equation 2*:

$$E = \frac{E^{*\,2}(1-\nu^2)}{E_i\,(1-\nu_i^2)} \qquad (Equation\ 2)$$

where E_i and ν_i are the elastic modulus and Poisson ratio, respectively, of the diamond tip nanoindenter, and ν is the Poisson ratio of the films. The elastic recovery parameter (ERP) is calculated according to *Equation 3:*

$$ERP = h_{max} - h_{plastic}/h_{max} \qquad (Equation\ 3)$$

where h_{max} is the maximum depth that the films were penetrated, and $h_{plastic}$ is the depth of the film that did not rebound after the indentation and is equal to 1 for a fully elastic deformation and equal to 0 for a fully plastic deformation. Complementary to ERP, the plasticity index (ψ) ranges from 0–1 and quantifies the plastic/elastic behavior of the films as they undergo indentation, with $\psi = 0$ for a fully elastic deformation, and $\psi = 1$ for a fully plastic deformation. Unlike the Instron and DMA tests, nanoindentation is a compressive test, and, furthermore, it probes beyond the elastic region of the stress-strain curve into the plastic.

The addition of glycerol reduced the hardness and modulus of the films (*Figs. 14A–B*). The res-CBD-CNC and CBD-CNC

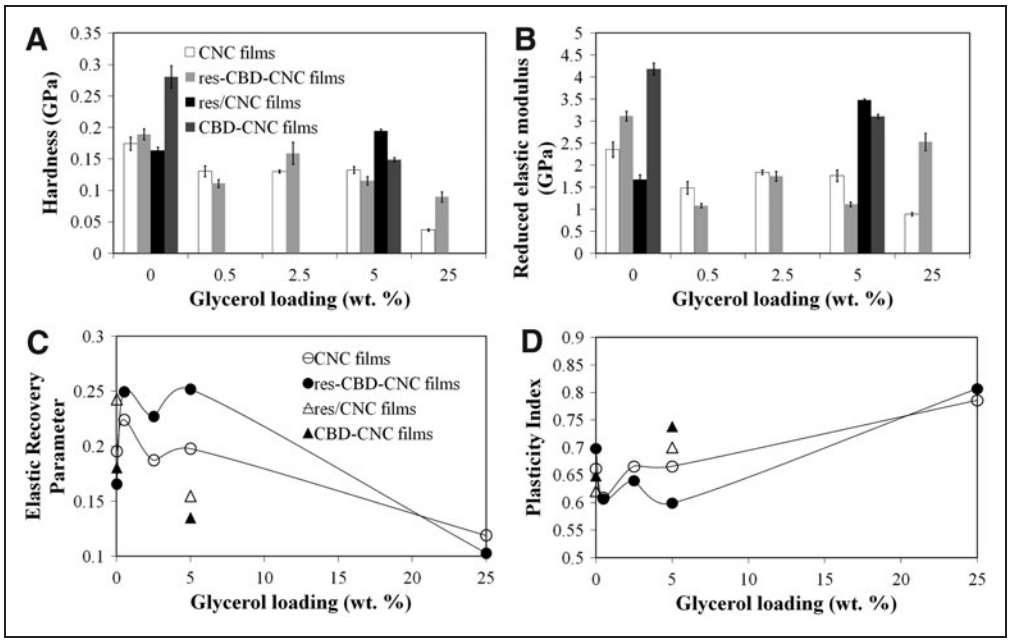

Fig. 14. Nanoindentation results (mechanical properties) of films measured as a function of glycerol loading: **(A)** hardness; **(B)** reduced elastic modulus; **(C)** elastic recovery parameter; and **(D)** plasticity index. The figure legends are indicated in **(A)** and **(C).** Dark gray bars/black filled triangles correspond to CBD-CNC films, white bars/open circles to CNC films, and gray bars/black filled circles to res-CBD-CNC films. Each data point is an average of 10 independent measurements, and error bars in **(A)** and **(B)** are calculated using a Student's t-test. The error bars in **(C)** and **(D)** were omitted since they approach the size of the data symbol, and the lines drawn are intended as visual guides.

films at 0 wt% glycerol had the highest hardness/modulus values, and as mentioned in the DMA discussion, this is most likely from a reinforcing interaction between res-CBD and CNCs and/or from CBD-induced alignment. At intermediate glycerol loadings (0.5–5 wt%) the hardness values and moduli of the CNC films generally surpassed the res-CBD-CNC films (except for hardness at 2.5 wt% glycerol), whereas the trend was reversed at 25 wt% glycerol. Possibly, the hardness/modulus differences reflect how easy it is for glycerol to flow from the compressed region; for instance, in the CNC films, the glycerol may be better able to flow upon compression, whereas res-CBD more closely involves the glycerol, making it harder for the glycerol to move away from the site of compression. If this is the case, upon compression, the CNC films are relatively desolvated compared to the res-CBD-CNC films, leading to harder and stiffer films at intermediate glycerol loadings. It is, however, unclear why the 25 wt% glycerol loading improved the hardness and modulus of the res-CBD-CNC film compared to the CNC film at the same glycerol loading.

It seems that the role of glycerol in the res-CBD-CNC films is different in *x-y* plane versus *z*-axis mechanical tests. In *x-y* plane tension (i.e., Instron and DMA tests), reinforcing interactions between glycerol-solvated res-CBD and CNCs are probed; specifically, at intermediate glycerol, reinforcement is observed, but at high glycerol, the reduction in CNC cohesion surpasses the reinforcement effect. Conversely, in *z*-axis compression (i.e., nanoindentation), the indentation encompasses stacks of CNC layers coated with soft glycerol layers (*Fig. 8*), and an overall reduction in the film hardness/compressive modulus is observed with added glycerol, which is more pronounced for res-CBD-CNC films compared to CNC films because of differences in how tightly glycerol is associated with the film components.

Of significant interest was whether res-CBD could impart some of the elastic properties of resilin to CNC films and, on a more fundamental level, whether aspects of elasticity could be conferred from non-crosslinked resilin. Similarly, what is the role of resilin solvation? *Figures 14C* and *14D* present the elastic recovery parameter and the plasticity index of the films. At 0 wt% glycerol, CNC and CBD-CNC films have a better elastic response compared to res-CBD-CNC films, whereas at intermediate glycerol loadings (0.5–5 wt%), res-CBD-CNC films are more elastic. At intermediate glycerol, res-CBD-CNC films and CNC films are more elastic than their glycerol-free counterparts, whereas the CBD-CNC film is less elastic at the 5 wt% glycerol loading that was studied. Overall, the res-CBD-CNC films at intermediate glycerol were the most elastic.

We tentatively ascribe the improvements in elastic behavior with intermediate glycerol loadings (for CNC and res-CBD-CNC films) to a lubricity effect stemming from the glycerol, which enables the films to better flow back into shape once the load has been removed. Furthermore, the magnitude of the improvement in elasticity in going from 0 wt% glycerol to films that contain up to 5 wt% glycerol is significantly greater for res-CBD-CNC films, suggesting that the partnership of res-CBD + glycerol gives the best elastic response. This is consistent with the picture of glycerol-loaded films under *z*-axis compression that was described above, i.e., since res-CBD interacts more closely with glycerol, res-CBD-CNC + glycerol films bounce back more readily after a compression, whereas the flow back of ''free'' glycerol in films that do not contain res-CBD is less extensive. In addition, the decrease in elastic response that was observed at 5 wt% glycerol for the CBD-CNC film (in contrast to the improved elasticity for the res-CBD-CNC film), further confirms that solvated resilin is responsible for the improved elastic response.

SUMMARY OF MECHANICAL TESTING

Overall, the mechanical behavior of the films is made up of contributions from each component, and the dominant contribution seems to depend to some degree on the direction of the load (*x-y* plane vs. *z* axis) and whether the test probes a local point (i.e., nanoindentation) or encompasses the entire length of the film (i.e., DMA and Instron). CNCs make up a stiff matrix, which in general seems to be softened by the addition of glycerol (*z*-axis compression and *x-y* plane tension), stiffened by the addition of CBD (*z*-axis compression and *x-y* plane tension), and either stiffened or softened by res-CBD, depending on whether the *x-y* plane or *z*-direction of the material was probed. The dependence of test methods (local versus global and compressive versus tensile) is explained by considering stiff CNC structures (mostly in the plane of the film, as seen in the SEM film cross-sections in *Fig. 8*) sandwiched by soft, solvated layers; in *x-y* plane tension, the film responds as a single entity the behavior of which depends on the strength of adhesion between hard and soft components, whereas in *z*-axis compression, the ease of flow from the site of the indentation determines the response. This work seems to indicate that uncrosslinked resilin tethered to CNCs via a CBD can confer some degree of elasticity to the films, especially when the resilin is solvated by glycerol; elasticity measurements from DMA and nanoindentation suggest improvements of $\sim$100 % for res-CBD films at 0.5 wt% glycerol compared to glycerol-free CNC and res-CBD-CNC films.

Conclusions

Resilin-CBD was successfully expressed, purified, and bound to cellulose nanocrystals prepared from the sulfuric acid hydrolysis of microcrystalline cellulose powder. Res-CBD-CNC films were compared to neat CNC films as a function of glycerol loading. The res-CBD-CNC films were more hydrophobic, exhibited long-range nematic particle orientation, and generally exhibited improved mechanical properties related to the presence of res-CBD and to glycerol-solvated res-CBD. The role of glycerol in the CNC films was that of a softener, whereas its effect on res-CBD-CNC films was more complex, leading to improved tensile properties (e.g., Young's modulus and storage modulus) and elastic response at intermediate loadings (0.5–5 wt%). Future work to better understand the role of glycerol in res-CBD-CNC materials, in particular crosslinked res-CBD-CNC materials, is currently underway, and in our view, may lead to functional bionanocomposites that have the potential to extend the elasticity of resilin to a wider range of conditions, such as increased temperatures and relatively dehydrated environments.

Acknowledgments

The authors thank Professors Y. Abraham, J. Moran-Mirabal, T. Hoare, and R. Pelton; the Biointerfaces Institute at McMaster University (Hamilton, Canada); and the McMaster Manufacturing Research Institute for laboratory and equipment access. Tiffany Abitbol is grateful to the Azrieli Foundation for the award of an Azrieli Fellowship.

Author Disclosure Statement

No competing financial interests exist.

REFERENCES

1. Habibi Y, Lucia LA, Rojas OJ. Cellulose nanocrystals: Chemistry, self-assembly, and applications. *Chem Rev* 2010;110(6):3479–3500.
2. Abitbol T, Kloser E, Gray DG. Estimation of the surface sulfur content of cellulose nanocrystals prepared by sulfuric acid hydrolysis. *Cellulose* 2013;20(2):785–794.
3. Mariano M, El Kissi N, Dufresne A. Cellulose nanocrystals and related nanocomposites: Review of some properties and challenges. *J Poly Sci B Poly Phys* 2014;52(12):791–806.
4. Buck ME, Tirrell DA. 9.07 - Artificial Proteins. In: Möller KM, ed. *Polymer Science: A Comprehensive Reference*. Amsterdam: Elsevier, 2012:117–136.
5. Maskarinec SA, Tirrell DA. Protein engineering approaches to biomaterials design. *Curr Opin Biotechnol* 2005;16(4):422–426.
6. Bailey K, Weis-Fogh T. Amino acid composition of a new rubber-like protein, resilin. *Biochim Biophys Acta* 1961;48(3):452–459.
7. Weis-Fogh T. A rubber-like protein in insect cuticle. *J Exp Biol* 1960;37:889–907.
8. Young D, Bennet-Clark H. The role of the tymbal in cicada sound production. *J Exp Biol* 1995;198(4):1001–1020.
9. Bennet-Clark HC, Lucey ECA. The jump of the flea: A study of the energetics and a model of the mechanism. *J Exp Biol* 1967;47(1):59–76.
10. Qin G, Hu X, Cebe P, Kaplan DL. Mechanism of resilin elasticity. *Nat Commun* 2012;3:1003.
11. Rånby BG. Aqueous colloidal solutions of cellulose micelles. *Acta Chem Scand* 1949;3(5):649–650.
12. Eichhorn SJ. Cellulose nanowhiskers: Promising materials for advanced applications. *Soft Matter* 2011;7(2):303–315.
13. Eichhorn SJ, Dufresne A, Aranguren M, et al. Review: Current international research into cellulose nanofibres and nanocomposites. *J Mater Sci* 2010;45(1):1–33.
14. Siqueira G, Bras J, Dufresne A. Cellulosic bionanocomposites: A review of preparation, properties and applications. *Polymers* 2010;2:728–765.
15. Azizi Samir MaS, Alloin F, Dufresne A. Review of recent research into cellulosic whiskers, their properties and their application in nanocomposite field. *Biomacromolecules* 2005;6(2):612–626.
16. Kalia S, Dufresne A, Cherian BM, et al. Cellulose-based bio- and nanocomposites: A review. *Int J Polym Sci* 2011;837875:1–35.
17. Klemm D, Kramer F, Moritz S, et al. Nanocelluloses: A new family of nature-based materials. *Angew Chem Int Edit* 2011;50(24):5438–5466.
18. Moon RJ, Martini A, Nairn J, et al. Cellulose nanomaterials review: Structure, properties and nanocomposites. *Chem Soc Rev* 2011;40(7):3941–3994.
19. Weis-Fogh T. Thermodynamic properties of resilin, a rubber-like protein. *J Mol Biol* 1961;3(5):520–531.
20. Abitbol T, Marway H, Cranston ED. Surface modification of cellulose nanocrystals with cetyltrimethylammonium bromide. *Nordic Pulp Paper Res J* 2014;29(1):046–057.
21. Qin G, Rivkin A, Lapidot S, et al. Recombinant exon-encoded resilins for elastomeric biomaterials. *Biomaterials* 2011;32(35):9231–9243.
22. Andersen S. The cross-links in resilin identified as dityrosine and trityrosine. *Biochim Biophys Acta* 1964;93:213–215.
23. Šturcová A, Davies GR, Eichhorn SJ. Elastic modulus and stress-transfer properties of tunicate cellulose whiskers. *Biomacromolecules* 2005;6(2):1055–1061.
24. Ardell DH, Andersen SO. Tentative identification of a resilin gene in *Drosophila melanogaster*. *Insect Biochem Mol Biol* 2001;31(10):965–970.
25. Elvin CM, Carr AG, Huson MG, et al. Synthesis and properties of crosslinked recombinant pro-resilin. *Nature* 2005;437(7051):999–1002.
26. Kim M, Elvin C, Brownlee A, Lyons R. High yield expression of recombinant pro-resilin: Lactose-induced fermentation in E. coli and facile purification. *Protein Expr Purif* 2007;52(1):230–236.
27. Qin G, Lapidot S, Numata K, et al. Expression, cross-linking and characterization of recombinant chitin binding resilin. *Biomacromolecules* 2009;10:3227–3234.
28. Rivkin A, Meirovitch S, Roth S, et al. *Bio-Inspired Elastic Composites of Nano Crystalline Cellulose and Cellulose Binding Resilin*. In: *34th Risø International Symposium on Materials Science: Processing of fibre composites - Challenges for maximum materials performance* 2013. Technical University of Denmark.
29. Verker R, Rivkin A, Zilberman G, Shoseyov O. Insertion of nano-crystalline cellulose into epoxy resin via resilin to construct a novel elastic adhesive. *Cellulose* 2014;21(6):4369–4379.
30. Goldstein MA, Takagi M, Hashida S, et al. Characterization of the cellulose-binding domain of the *Clostridium cellulovorans* cellulose-binding protein A. *J Bacteriol* 1993;175(18):5762–5768.
31. Dong XM, Revol JF, Gray DG. Effect of microcrystallite preparation conditions on the formation of colloid crystals of cellulose. *Cellulose* 1998;5(1):19–32.
32. Truong MY, Dutta NK, Choudhury NR, et al. The effect of hydration on molecular chain mobility and the viscoelastic behavior of resilin-mimetic protein-based hydrogels. *Biomaterials* 2011;32(33):8462–8473.
33. Boraston AB, Bolam DM, Gilbert HJ, Davies GJ. Carbohydrate-binding modules: Fine-tuning polysaccharide recognition. *Biochem J* 2004;382(3):769–781.
34. Tormo J, Lamed R, Chirino AJ, et al. Crystal structure of a bacterial family-III cellulose binding domain: A general mechanism for attachment to cellulose. *EMBO J* 1996;15(21):5739–5751.
35. Linder M, Teeri TT. The roles and function of cellulose-binding domains. *J Biotechnol* 1997;57:15–28.
36. Dutta NK, Choudhury NR, Truong MY, et al. Physical approaches for fabrication of organized nanostructure of resilin-mimetic elastic protein rec1-resilin. *Biomaterials* 2009;30(28):4868–4876.
37. Beck S, Bouchard J, Berry R. Dispersibility in water of dried nanocrystalline cellulose. *Biomacromolecules* 2012;13(5):1486–1494.
38. Majoinen J, Kontturi E, Ikkala O, Gray D. SEM imaging of chiral nematic films cast from cellulose nanocrystal suspensions. *Cellulose* 2012;19(5):1599–1605.
39. Revol JF, Bradford H, Giasson J, et al. Helicoidal self-ordering of cellulose microfibrils in aqueous suspension. *Int J Biol Macromol* 1992;14(3):170–172.
40. Revol JF, Godbout L, Dong XM, Gray DG. Chiral nematic suspensions of cellulose crystallites; Phase separation and magnetic field orientation. *Liq Cryst* 1994;16(1):127–134.
41. Dong XM, Gray DG. Effect of counterions on ordered phase formation in suspensions of charged rodlike cellulose crystallites. *Langmuir* 1997;13(8):2404–2409.
42. Pan J, Hamad W, Straus SK. Parameters affecting the chiral nematic phase of nanocrystalline cellulose films. *Macromolecules* 2010;43(8):3851–3858.
43. Revol JF, Godbout DL, Gray DG. 1997. Solidified liquid crystals of cellulose with optically variable properties. US Patent Application No. CA2182387.
44. Revol JF, Godbout L, Gray DG. Solid self-assembled films of cellulose with chiral nematic order and optically variable properties. *J Pulp Pap Sci* 1998;24(5):146–149.
45. Mu X and Gray DG. Formation of chiral nematic films from cellulose nanocrystal suspensions is a two-stage process. *Langmuir* 2014;30(31):9256–9260.

46. Araki J, Kuga S. Effect of trace electrolyte on liquid crystal type of cellulose microcrystals. *Langmuir* 2001;17(15):4493–4496.

47. Abitbol T, Cranston ED. Chiral nematic self-assembly of cellulose nanocrystals in suspensions and solid films. In: Oksman K, ed. *Handbook of Green Materials: World Scientific* 2014:37–56.

48. Abraham Y, Elbaum R. Quantification of microfibril angle in secondary cell walls at subcellular resolution by means of polarized light microscopy. *New Phytol* 2013;197(3):1012–1019.

49. Abitbol T, Cranston ED. Directed assembly of oriented cellulose nanocrystal films. In: Oksman K, ed. *Handbook of Green Materials: World Scientific* 2014:79–103.

Address correspondence to:
Tiffany Abitbol
Postdoctoral Fellow
Robert H. Smith Faculty of Agriculture, Food and Environment
The Hebrew University of Jerusalem
POB 12
Rehovot 76100
Israel
Phone: 972-8-9489083

E-mail: tiffany.abitbol@mail.mcgill.ca